



Engineering geomorphological reconnaissance of the December 2018 Waimata Valley mud volcano eruption, Gisborne, New Zealand

Alex Leighton¹, Martin S. Brook^{1*}, Murry Cave², Michael C. Rowe¹, Alec Stanley¹ and Jon F. Tunnicliffe¹

¹ School of Environment, The University of Auckland, Auckland 1010, New Zealand

² Gisborne District Council, Gisborne 4010, New Zealand

AL, 0000-0001-9395-0109; MSB, 0000-0002-1030-3246; MCR, 0000-0002-8052-2882; AS, 0000-0002-6563-2258; JFT, 0000-0003-0377-7803

*Correspondence: m.brook@auckland.ac.nz

Abstract: Gisborne (North Island, NZ) is affected by rainfall-induced landslides, earthquakes and tsunami, as well as mud volcanoes (MVs). The latter form via upward mobilization of Eocene-age sediments, and have not been studied from an engineering geological standpoint, so the 15 December 2018 Waimata Valley MV eruption provided a unique opportunity. The event erupted c. 16 900 m³ of mud, forming an elevated vent area, and three mudflows propagating north, east and south. Scanning electron microscopy (SEM) identified smectite as the dominant clay in the Sr-rich mud, and Atterberg limits indicate high plasticity. In-situ testing using dynamic cone penetrometer and shear vane (3–168 kPa) revealed wide variability in strength properties with depth, while ring shear values are 11.3–13.5°. A fault extends NW beneath the Waimata Valley MV, coinciding with the pre-existing Arakihi Road MV. The Waimata Valley MV area was subject to uplift and cracking during the September 2016 Te Araroa earthquake (M_w 7.1), which caused increased activity at pre-existing mud volcanoes at that time. Geodetic data for the Gisborne district shows an uplift phase culminating around the December 15 2018 MV eruption, followed by the commencement of a Hikurangi subduction zone ‘slow slip event’. Nevertheless, relationships between tectonics and MV eruptions remain equivocal.

Received 19 October 2021; revised 21 March 2022; accepted 26 May 2022

Mud volcanoes (MVs) are the surface expression of sediment remobilization and focused fluid flow, and are one example of natural hydrocarbon seepage structures and natural gas venting systems (Kopf 2002; Deville 2009; Mazzini and Etiope 2017; Blouin 2019). MVs are characterized by localized expulsion of argillaceous material remobilized from the subsurface associated with high fluid pressures, gas exsolution, and the buoyant force of a low-density source layer (Kopf 2002; Deville 2009; Blouin *et al.* 2019; Odonne *et al.* 2020). This mud expulsion is driven by the mobilization of fluids (e.g. water and oil) and gas resulting from compaction, diagenetic transformation and thermal maturation of sediments (Brown 1990; Deville *et al.* 2003; Odonne *et al.* 2020), or some combination of these processes. Such mud emissions tend to be episodic phenomena, with eruptive phases typically less than a few days, separated by quiescent intervals that can persist for decades (Mazzini and Etiope 2017). Mud volcanoes are broadly distributed throughout the globe both onshore and offshore in active margins, passive margins, deep sedimentary basins related to active plate boundaries, as well as delta regions, or areas involving salt diapirism (Miljkov 2000; Dimitrov 2002; Kopf 2002; Mazzini and Etiope 2017). They range in size from meter-size cones to edifices a few hundred meters high that extend laterally a few kilometres (Vona *et al.* 2015; Mazzini and Etiope 2017). Fundamentally, MVs are located in petrolierous basins and are part of petroleum systems (Etiope 2015; Mazzini and Etiope 2017, p. 83). The exact definition of a MV has been a topic of recent debate. For example, since 2006 the ongoing Lusi catastrophe in Indonesia has destroyed 15 villages, displacing >40 000 people and causing c. US\$3 billion in damage, is exceedingly well monitored and studied, but the triggering processes of the eruption are still debated (e.g. Tingay *et al.* 2017). However, while Lusi has been widely described as a MV by many

workers (e.g. Tingay *et al.* 2017) due to a (drilling related) triggering mechanism of high overpressure and gas influx into weak layers, Mazzini and Etiope (2017) disagree. Indeed, Mazzini and Etiope (2017) outline that Lusi is not a MV, but rather a sediment-hosted hydrothermal system, noting the high geothermal gradient (42°C/km), unlike the typical sedimentary basins where MVs are common.

Notwithstanding the conjecture regarding precise terminology, mud volcanism does represent one of the most intriguing phenomena of the Earth’s crust, as these structures are not currently well understood or explained (Kopf 2002; Mazzini and Etiope 2017). Indeed, mud volcanism remobilizes compacted sediments while fluidizing them through physical cold processes (Deville *et al.* 2003; Mazzini and Etiope 2017). Moreover, mud volcanism has direct implications for energy resource exploitation (Magoon and Schmoker 2000), seismicity (Kopf *et al.* 2010), atmospheric budgeting of greenhouse gases (Etiope 2015), and geohazard zonation (Madonia *et al.* 2011). Indeed, MVs can represent a geohazard for several reasons. First, potentially violent releases of large amounts of hydrocarbons and mud can occur, for example the Maccalube tragedy in Italy in 2014 (Vona *et al.* 2015), and these can include igniting methane, as well as highly mobile mud flows. Second, many MVs have craters and muddy pools that are easily accessed by the public, and while the craters may only be <1 m wide, they can be >2–3 m deep, representing a dangerous trap; such pools can also undermine foundations (Etiope 2015). Existing settlements may also be unwittingly located on pre-historic larger, thick erupted mud breccia flows, which can pose hazardous if liquefaction occurs due to seismic activity (Mazzini and Etiope 2017). Third, MVs are often associated with locations where offshore gas hydrates are exploited, and gas exsolution can lead to pockmark formation, while overpressure issues for drilling

platforms and pipeline corridors (e.g. Guliyev *et al.* 2001). Moreover, the activity stage of MVs (which can evolve at different speeds) presents a further problem, because the features can be in either eruptive, dormant/sleeping, extinct, or fossil phases (Mazzini *et al.* 2009). Thus, even though MVs are mostly considered harmless tourist attractions, their hazard should be evaluated, in particular in those localities where sudden eruptions have occurred in proximity to property and infrastructure, such as the Lusi eruption (e.g. Tingay *et al.* 2017).

In this work, we present results from a field reconnaissance and preliminary laboratory investigation of a mud eruption (38.491°S, 178.059°E) that occurred 15 December 2018 in the Waimata Valley 19 km north of Gisborne on New Zealand's North Island (Fig. 1). Located within the Hikurangi Subduction Zone, Gisborne has long been recognized as an area subject to mega-thrust earthquakes, tsunami, severe erosion, landslides and flooding (Mazengarb and Speden 2000). Quiescent and paroxysmally eruptive mud volcanoes are present in the region and extrude Eocene–age bentonitic muds with a few boulders from beneath Neogene sedimentary rocks, of total thickness of c. 6100 m (Ridd 1970). New residential development is occurring in Gisborne's Wheatstone Road area, where a dormant MV is located (it was active as recently as 2007), and where inflammable gas expulsion and ground cracking occurred in 1931 (Strong 1933). Hence, the 2018 Waimata Road eruption provides a rare opportunity to document and interpret the eruption cycle, geomorphic processes, material properties of a mud volcano, and to assess the geological conditions controlling eruption activity.

Study area

The Waimata Valley MV is situated within the Gisborne district (Fig. 1a, b), in gently rolling to moderately steep hill country

roughly NNE from the town of Gisborne. More than 250 fluid and/or gas seeps and at least 4 oil seeps have been reported within the east coast region of the North Island (e.g. Field *et al.* 1997). Some of these seeps are associated with diapiric mud extrusion along the fault zones in the Hikurangi margin (Fig. 1a), both onshore and offshore (Pettinga 2003). In spite of these numerous seep localities, there are few reports documenting mud volcanism in the region. Exceptions are Pettinga's (2003) description of a MV that erupted a decade prior, and Nelson and Healy's (1984) delineation of an area of pock-marked sea floor in Poverty Bay, off Gisborne. Pockmarks fundamentally differ from MVs in that they are erosional features forming relatively shallow seabed depressions in soft, fine-grained sediments by fluid (water or gas expulsion) into the water column (Judd and Hovland 2007; Chen *et al.* 2015). The 2018 Waimata Valley MV (locally called the 'Utting's MV') is shown in Figure 1c, in addition to two other known MVs active during the early twentieth century, as reported by Ridd (1970). In particular, the Mangaehu Stream (locally, 'Savage's MV') MV 3.5 km SW of the 2018 Waimata MV (Fig. 1c) showed significant eruptive activity from 1908 onwards (Adams 1908; Ridd 1970). The 1908 MV in the Mangaehu Stream was mistakenly stated by Kopf (2002, p. 44) to have occurred 3.5 km NE, in the Waimata Valley. The 2018 Waimata Valley MV is located at the northern end of the Waimata Valley, c. 19 km north of Gisborne (Fig. 1c). It occupies the boundary between two sheep and cattle farms, owned by the Hall family to the north, and by the Utting family to the south. The Hall's farmstead is located c. 250 m north of the MV. The site is located near the boundary of the two farms, on terrain sloping gently between 5–10° to the north and south (Fig. 2). The MV (Fig. 1c) lies c. 50 m to the west of the boundary between the early Pliocene Mangaheia Group siltstone and sandstone (ePmz) and the much older, Eocene Mangatua Group

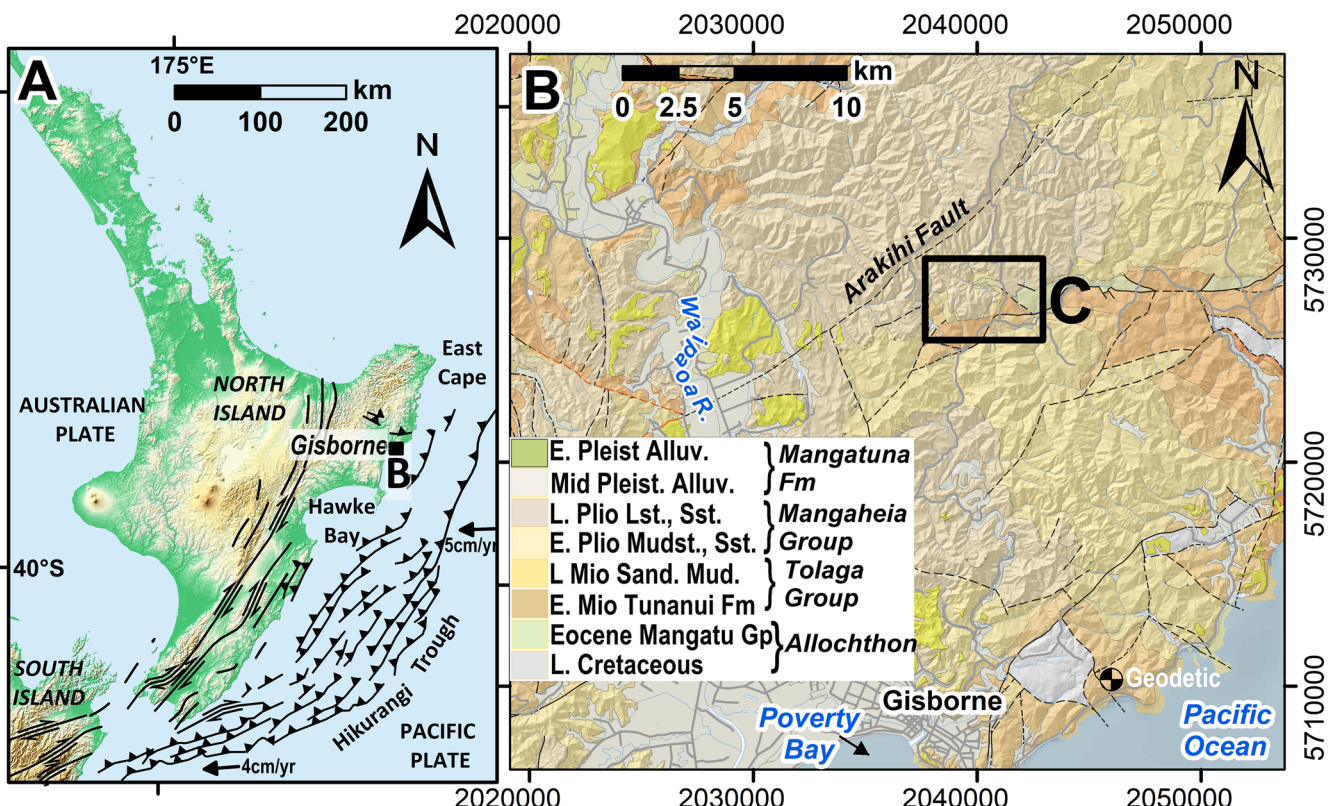


Fig. 1. (a) Location of Gisborne on the North Island and major structures of the obliquely convergent Hikurangi margin, (b) regional geology and geomorphology of the broader area. The site is 20 km north of Gisborne south of the Arakihi Fault, (c) geomorphology and geology of the area, including existing mud volcanoes. The general geomorphology of the area reflects the complexity of the underlying inclined and faulted sediments (see text for abbreviations). The 15 December 2018 mud volcano is 100 m east of Waimata Valley Road, and 800 m east of Mangahouku Stream. Coordinate systems are New Zealand Transverse Mercator (NZTM).

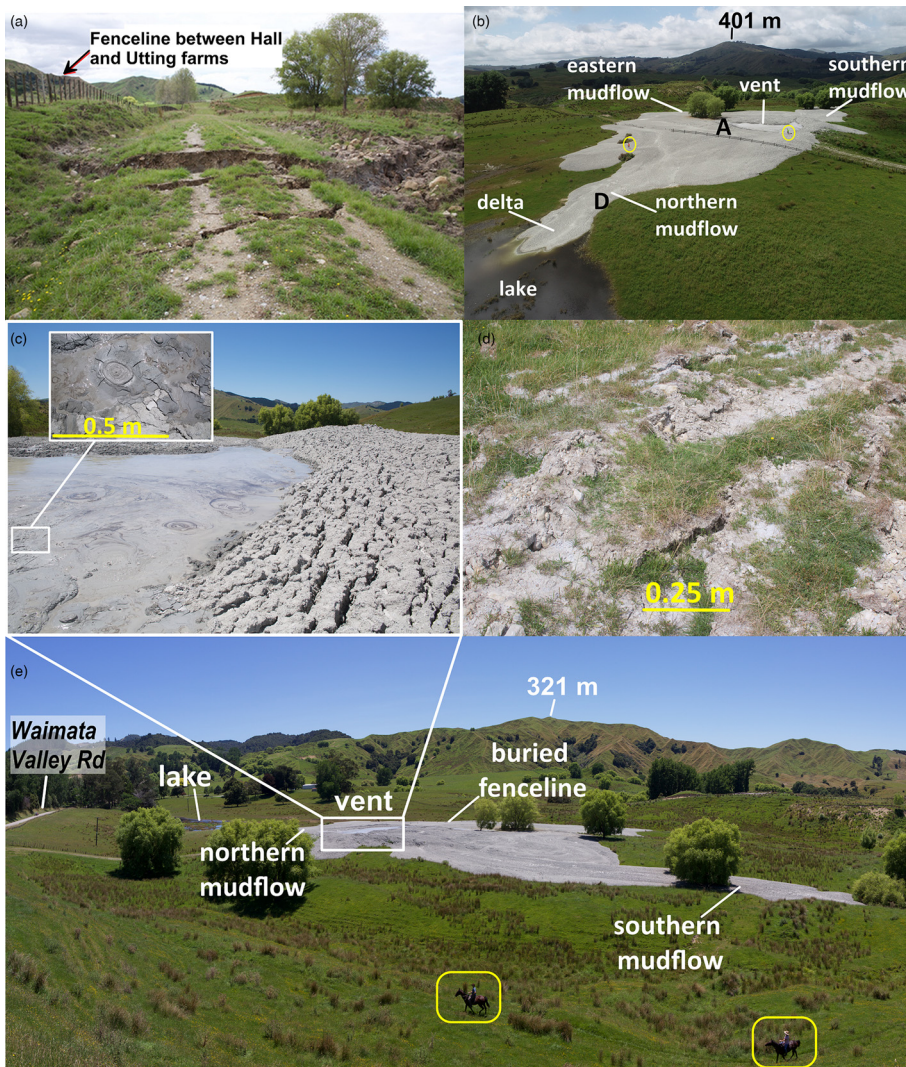


Fig. 2. (a) Surface rupturing following the 2 September 2016 Te Araroa earthquake (M_w 7.1), (b) view SE on 6 January 2019, following mud volcano eruption (buried fence line in black and people circled for scale), (c) vent area and rim on west side), (d) tension cracks around margin, (e) view NE 6 January 2019 (horse riders highlighted by yellow boxes for scale).

mudstone (Egw). Present to the south and west are Miocene Tolaga Group sediments, including early Miocene mudstone and tuff (eMt), mid-Miocene mudstone and tuff (mMt), and Miocene mudstone, sandstone and tuff (IMt). Holocene colluvium and alluvium deposits are also present on the hillsides and river valleys (Fig. 1c). A fault intersects both the Waimata valley MV and the existing Arakihi Road MV, 600 m to the NW. The fault is normal, with the Eocene Wanstead Formation on the east side downthrown against undifferentiated Miocene Tolaga Group on the west. The site of the 2018 Waimata Valley MV was ruptured during the 2 September 2016 M_w 7.1 Te Araroa earthquake (Fig. 2a). The mud volcano erupted on 15 December 2018, blanketing the area with a thick mud slurry that flowed to the north and south of the vent, over distances of up to 160 m (Fig. 2).

Methods

Aerial Surveys

A range of complementary approaches were implemented to investigate the mud volcano's material properties and geomorphic characteristics. Remote sensing in the form of airborne LiDAR and an unmanned aerial vehicle (UAV) survey were used to assess the terrain and geomorphic processes. The LiDAR data was collected on 15 February 2019 in the course of the region-wide Tairawhiti District Survey, from a fixed wing aircraft using an Optech Galaxy PRIME LiDAR system. The survey had a point density of 4 points per m^2 , horizontal accuracy of ± 1 m and vertical

accuracy of ± 0.2 m. The UAV survey was undertaken with a DJI Phantom 4 Pro in December 2018 following the eruption, using only the uncorrected UAV GPS information for georeferencing. The UAV survey data was processed in Pix4D Mapper using the structure-from-motion (SfM; James *et al.* 2017) technique to provide a seamless georeferenced photomosaic image of the site as a base map for geomorphological mapping.

Engineering properties

Soil sampling was attempted at several locations across the mud volcano (Fig. 3) following the guidelines summarized by Roberts *et al.* (2017), using hand augers (HA#) and test pits (TP#), but significant core loss occurred with some of the hand augers. A Scala dynamic cone penetrometer (e.g. Gabr *et al.* 2001) was used to evaluate the strength of the subsurface. This method uses a 9 kg hammer dropping through a height of 510 mm to drive a 60° cone into the subsurface. The number of blows required to drive the cone 100 mm are then recorded at different depths. Field shear strength was also estimated using a Geotechnics handheld field shear vane. Following the New Zealand Geotechnical Society guideline (NZGS 2001), the shear vane blade was inserted into the mud volcano to a depth at least twice the length of the vane blade, and extension rods were used to measure at different depths in the auger holes, as the hole was advanced. Both undisturbed (S_u 'peak') and disturbed (S_d ; 'residual') shear vane strength were recorded (in kPa). Samples were taken for laboratory analysis of

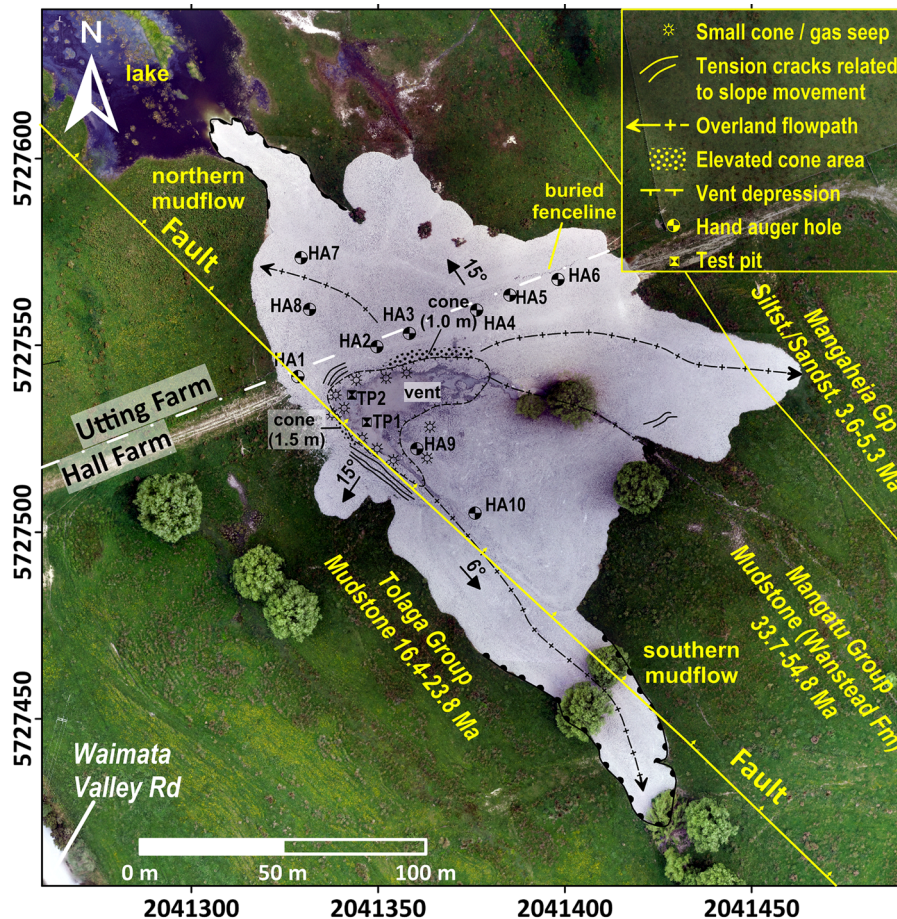


Fig. 3. Engineering geomorphological map of mud volcano and hand auger and test pit sample sites. Coordinate system is New Zealand Transverse Mercator (NZTM).

particle size, water content, and Atterberg limits. Samples were oven-dried to 105°C, sieved to remove the coarse fraction, and subsampled for particle-size distribution analysis using a Malvern Mastersizer 2000. Sample preparation involved placing c. 10 g of sample into a test tube with 20 ml of 10% sodium hexametaphosphate (Calgon), a dispersant solution to aid disaggregation of the individual clay particles (Blott *et al.* 2004). Test tubes containing the samples were then placed in an ultrasonic bath for 5 minutes to further improve accuracy of the testing. The Atterberg limits were obtained on the <0.425 µm fraction of the soils using a Casagrande cup, following BS 1377-2 (1990). Soil dispersion potential (when soil aggregates collapse upon wetting) was investigated using the Emerson class number (ECN), following the procedures outlined in AS 1289.3.8.1 (Standards Australia 2006). Ring shear testing of selected samples was determined using a Wykeham Farrance Annual Ring Shear apparatus (e.g. Meehan *et al.* 2007).

Mineralogy

Additional soil samples were collected to identify clay minerals and microtexture using a FEI Quanta 200 field emission environmental scanning electron microscopy (ESEM). Trace element abundances in the separated clay-size fraction were analysed from clays from the Waimata mud volcano, and three other local mud volcanoes (Fig. 1c), together with 15 additional non-volcano sediment sites within the Mangaehu catchment. Clay-sized particles were separated by centrifuge and dried to glass slides for chemical analysis using a laser ablation inductive coupled plasma mass spectrometry (LA-ICPMS) at the University of Auckland. Analyses were conducted on an Agilent Technologies 7700 Series ICPMS with a 193 nm ASI Resolution laser ablation (LA) system.

Results

Geomorphology

The characteristic geomorphological features of the mud volcano are shown in photographs (Fig. 2) and in an engineering geomorphological map (Fig. 3). Topographic changes are shown in Figure 4, including an indicative cross-section NW-SE across the MV. The MV (area c. 11 500 m², volume c. 16 900 m³) is characterized by a slightly elevated vent area (c. 530 m²) in the west-central part of the feature, with three distinct mud flows or 'fingers' propagating from the vent to the north, east and south (Fig. 2b). These flows are topographically constrained, in-part, by pre-existing gullies and depressions. The mud volcano is centred on the topographic bulge that appeared during the September 2016 Te Araroa earthquake (Fig. 2a). The erupted materials are fines with occasional gravels visible in areas distal to the vent. An elevated cone edifice accreted c. 1.5 m above the western side of the vent (Fig. 2c), because westward flow was constrained by the slope. The vent area (c. 500 m²) is a zone of fluidized mud, with methane and saline fluids emanating via regular seeping every 10–30 seconds (Fig. 2c). The area adjacent to the vent is characterized by desiccation cracks. The north flow terminates c. 40 m from the vent margin, and has a surface gradient of c. 15°, consistent with the underlying pre-eruption slope. This flow dammed the stream that previously flowed through the site, forming a 6050 m² lake (Figs 3, 4). The southern flow extends the furthest (c. 140 m) from the vent with a surface gradient of 6°, extending along an existing stream channel, and inundating the lower trunks of several trees (Figs 2e, 3). Several preferential surface flow paths formed across the MV surface, transporting meteoric water as well as vent fluids towards the margins, scouring shallow (<0.5 m deep) channels. Low scarplets from slumping material and tension

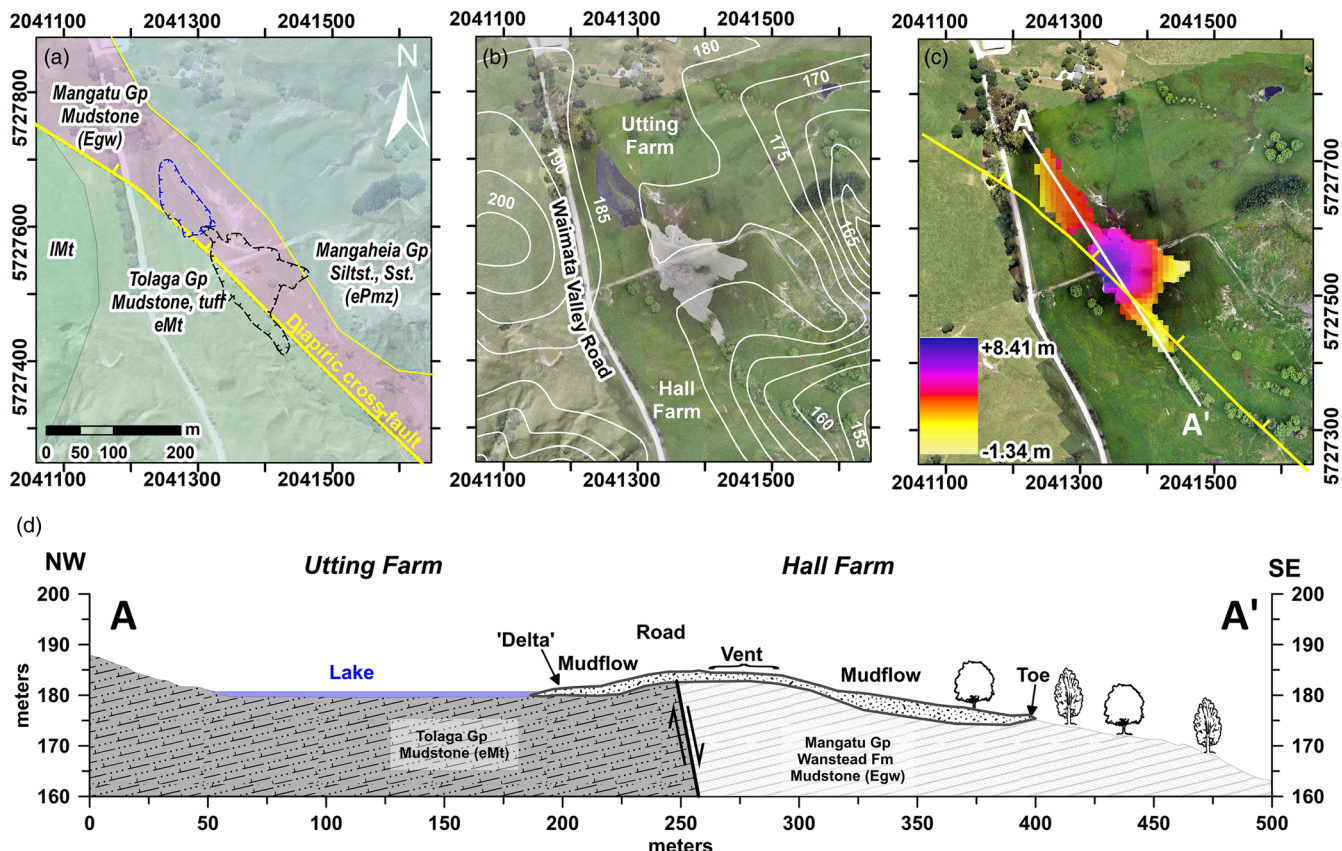


Fig. 4. (a) Pre-eruption aerial image with geology, mud volcano (black) and lake (blue) superimposed, (b) post-eruption aerial image with 5 m contours, (c) DEM-difference map showing the change in elevation from pre-2016 to 2019, including the effects of both the 2016 earthquake-induced uplift and the 2018 mud volcano eruption; and (d) long-section with indicative near surface geology. Coordinate system is New Zealand Transverse Mercator (NZTM)).

cracks are visible on the southwestern side of the vent area, where the material was remobilized and deformed along a 15° surface gradient. A fault trace visible to the SE extends NW, underneath the MV (Figs 3, 4) and is the likely linear source for the expelled mud. Notably, the Arakihi Road MV (locally, ‘Hall’s MV’) field also emerges along the same fault line NW of this site (Fig. 1c). The September 2016 earthquake and uplift, coupled with the accretion from the December 2018 MV eruption, has led to an overall c. 8 m gain in topographic elevation at the site (Fig. 4).

Material properties

In situ engineering properties

Summary descriptions of the lithological characteristics and *in situ* strength properties are reported in Table 1, with sampling locations shown in Figure 4. A summary of laboratory testing results is provided in Table 2. Across the MV, ten hand auger holes and two test pits were attempted. Across the site a distinct whitish-grey, dried

crust had formed, 0.1–0.2 m thick, and stiff enough to be traversed by foot, apart from the vent area. The crust comprised a very fine matrix of silt and clay with occasional clasts ranging from sand to boulder-sized. The silty-clay sized mud below the crust exhibited a high moisture content and, from the soil augering, extended to depths of c. 2.8 m. Below 2.8 m depth, the subsurface topsoil and alluvium was encountered around the margins of the volcano.

Mineralogy

LA-ICPMS (Fig. 5) and SEM photos (Fig. 6) highlight the geochemistry and mineralogy of the eruptive materials. In particular, the LA-ICPMS analyses (Fig. 5) show that clay-sized particles from the four sampled MVs in the region contain significantly higher concentrations of Sr (140–505 ppm; mean 345 ppm) when compared to clays from other locally-derived sediments (30–137 ppm; mean 80 ppm). Other analysed trace elements have similar abundances between the MV and catchment

Table 1. Lithological descriptions of soils encountered in the mud volcano

Depth range (m)	Lithology	Geotechnical description	Ave. DCP n / 10 cm	S _u kPa	S _d kPa	SI
0.1–0.2	Dried crust	Silty CLAY, stiff, dry, slightly plastic; some mudstone gravel. Hardened surficial crust due to drying of expelled mud.	0.6	45–168	8–17	5.6–9.9
0.2–2.8	Mud	Silty CLAY, with trace mudstone gravel; very soft, moist-wet high plastic. Expelled mud existing at natural moisture content.	0.5	3–25	2–7	1.5–3.6
>2.8	Buried topsoil / alluvium	CLAY, minor silt, minor organics; greyish brown; firm, moist-wet, moderately plastic; organics, fibrous and amorphous. Topsoil and alluvium prior to eruption.	1.5	45–109	11–33	3.3–4.1

DCP, Scala dynamic cone penetrometer; S_u, undisturbed shear vane; S_d, disturbed shear vane

Table 2. Soil index properties and ring shear testing of selected mud volcano samples

Sample	w_L (%)	w_P (%)	I_P (%)	w (%)	I_L (%)	I_C	D_{10} (μm)	Clay (%)	Activity	ϕ_r ($^\circ$)	ECN
TP1	56.0	22.8	33.2	82.4	1.8	-0.8	0.06	16.5	2.0	13.5	4/5
TP2	57.7	24.1	33.6	77.7	1.6	-0.6	0.05	19.9	1.7	-	-
HA3	65.7	24.3	41.4	54.4	0.7	0.3	0.04	27.2	1.5	11.3	-
HA4	55.1	25.3	29.8	56.6	1.1	-0.1	0.05	19.3	1.5	-	-
HA8	63.2	24.0	39.2	48.2	0.6	0.4	0.04	24.0	1.6	-	4/5
HA10	55.5	24.0	31.5	51.9	0.9	0.1	0.07	14.2	2.2	-	-

w_L , liquid limit; w_P , plastic limit; I_P , Plasticity Index; w , water content; I_L , Liquidity Index; I_C , Consistency Index; ϕ_r , residual friction angle; ECN, Emerson class number

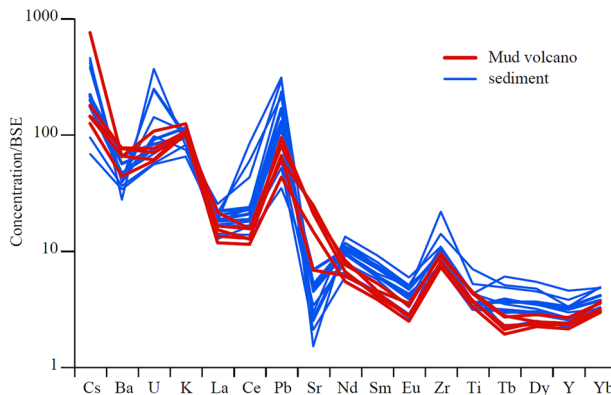


Fig. 5. Trace element abundance in the separated clay-size fraction using laser ablation inductive coupled plasma mass spectrometry (LA-ICPMS) for mud volcano samples, and surface sediment exposures.

samples, while Cs shows high variability across the four MVs (Fig. 5). Some trace elements (U, Zr and Pb) are more abundant in the catchment sediment samples, than from mud volcanoes (Fig. 5). Imaging of the soil samples under SEM (Fig. 6) confirmed the presence of smectite, which is a dominant clay in the region. Other features visible in the SEM analyses included pyrite and sphalerite, indicating the source mud rocks contained dissolved base metals. Desiccation cracks were also visible due to post-deposition shrinkage.

Laboratory-derived engineering properties

Table 2 and Figure 6 summarizes the soil index properties of the mud samples obtained from the test pits and hand augers. The in-situ moisture content (w) of the samples ranged from 48.2 to 82.4%, with the test pit samples closest to the vent displaying the highest moisture content. The plastic limits (w_P) of the samples were consistent across the site, ranging from 22.8 to 25.3%, and the liquid limit (w_L) ranged from 55.1 to 65.7%. Therefore, all samples exhibit high plasticity and can be classified as ‘fat clays’ (CH), following ASTM D2487 (Fig. 6a). An assessment of particle-size distribution was performed on samples from both hand auger holes and test pits. Prior to testing in the Mastersizer apparatus, the proportion of the gravels removed ($>2 \text{ mm}$) was determined to range from 1% to 3% (by mass). The effective particle size (D_{10}) was $<0.1 \mu\text{m}$ for all samples (Table 2; Fig. 6b) For all of the samples the percentage of fine fraction ($<60 \mu\text{m}$) exceeds 35%, so the soils can be described as cohesive. Indeed, the distribution curve (Fig. 6b) shows that the soils are dominated by silt-sized fractions and finer (51–81%), with a significant proportion within the clay range (10–27%). The percentage clay fraction and the I_P (plasticity index) were plotted together according to Skempton’s (1953) activity index (AI), which is defined as the ratio of the I_P to the percentage clay-sized fraction (Fig. 6c). Following Skempton (1953), all the samples are classed as ‘active’ to ‘highly active’. Most samples have a liquidity index (I_L)

of 0 to 1, so their natural water content is greater than the plastic limit (Table 2). However, the samples from the vent area both have liquidity indices (I_L) >1 , reflecting that those samples were in a liquid state. The consistency index (I_C) values varied from -0.8 to 0.4, again, indicating that the vent area samples have a natural water content that is greater than the liquid limit, with resultant fluid-like behaviour ($I_C < 0$).

The dynamic cone penetrometer (Scala) results varied from an average blow count of 0.6/100 mm at the surface to 1.5/100 mm below 2.8 m. Thus, the mud would be classed as ‘very loose’ according to the NZGS (2005) relative density index. Following the Stockwell (1977) classification chart, the material is inferred to have an allowable bearing capacity (q_a) of c. 20 kPa, classed as ‘very soft’. The undisturbed (S_u) shear vane test gave values of 3–168 kPa, with the disturbed shear vane (S_d) results ranging from 2 to 33 kPa. In particular, the surface samples (dried crust) are typically firm to very stiff, while below 0.2 m depth, the mud is softer than the surficial crust, until the underlying topsoil is encountered at $>2.8 \text{ m}$ (Table 1). Given these S_d and S_u values, the sensitivity index (SI) of the soils ranges from 1.5 to 9.9 (Table 1), with the surface crust classed as ‘sensitive’ to ‘extra sensitive’, following Skempton and Northey (1953). The mud below the crust and the topsoil underlying the MV deposit are ‘low’ to ‘medium’ sensitivity (Table 1). Soil reactive properties were also estimated using the Emerson class numbers (ECN), and while no colloidal cloud developed, slaking did occur, indicating the presence of montmorillonite and illite (ECN 4/5). The residual friction (ϕ'_r) from ring shear tests of two samples were 11.3° (augered sample of mud) and 13.5° (surficial dried crust; Table 2). These low friction angles are typical of clayey, smectite-rich soils, where in a residual state, platy clay minerals are preferentially oriented (e.g. Gibo *et al.* 1987). The ring shear tests indicate the soils are of low residual strength and are vulnerable to remobilization due to meteoric water input and groundwater changes. In undrained conditions, the factor of safety (F) against shear failure for an infinite slope is given by the formula (e.g. Barnes *et al.* 2010):

$$F = \frac{C_u}{\gamma z \cos \beta \sin \beta} \quad (1)$$

where C_u is undrained shear strength of soil, γ unit weight of soil (17 kN/m³), z is soil thickness (2 m), β is slope angle (6°). The net resisting force (3.28) and net driving force (3.53) results in $F = 0.93$. Therefore, even with a slope angle of c. 6°, the factor of safety (F) is <1 , this means that following prolonged rainfall, the MV material may deform and remobilize downslope, even on very low gradients (<6°).

Discussion

Material properties

The particle-size distribution of material ejected from similar MVs around the world (e.g. Yassir 1989; Kopf 2002; Deville 2009;

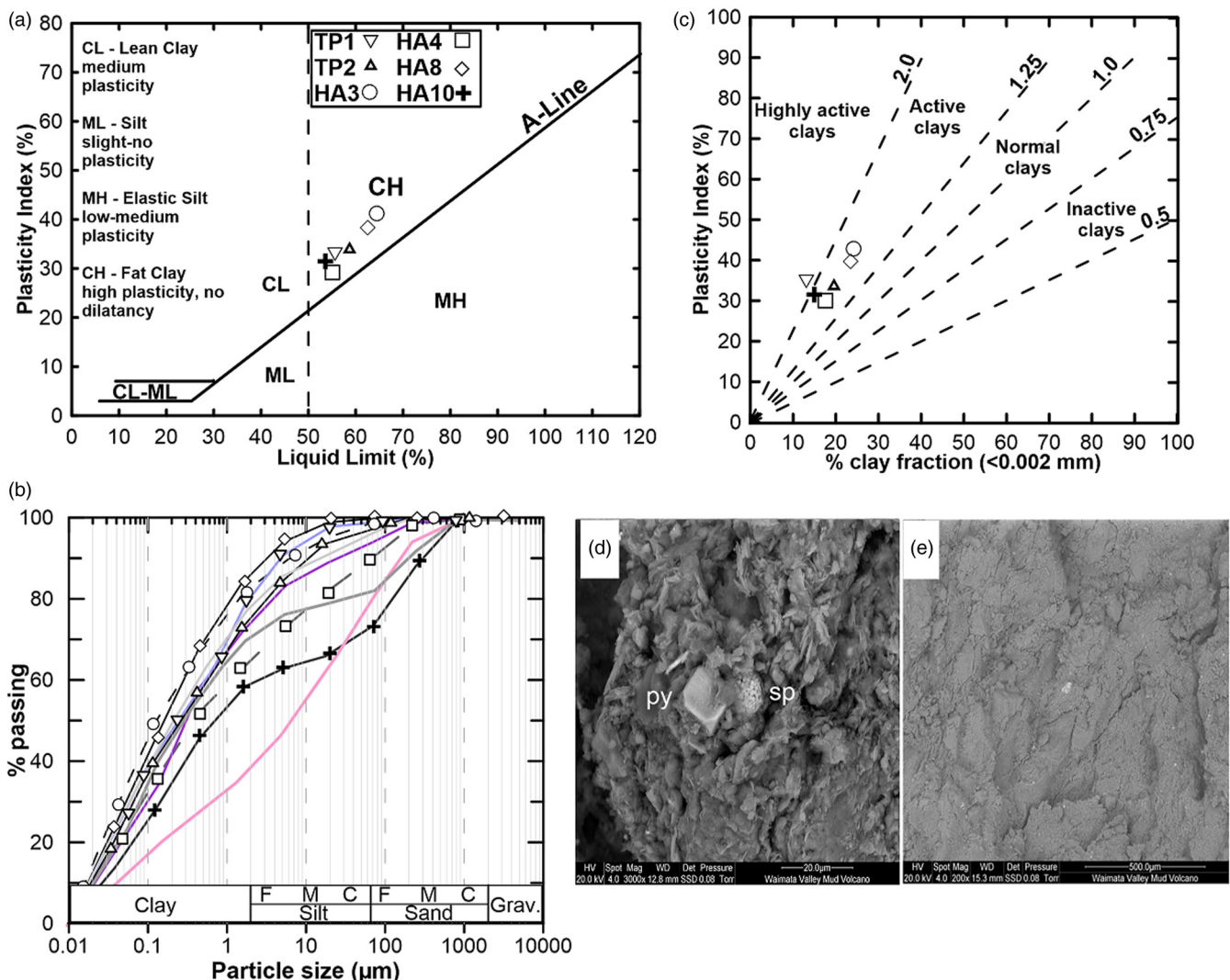


Fig. 6. Engineering and mineralogical properties of Waimata mud volcano soil samples, including (a) Casagrande plasticity chart, A-line based on NZGS (2005), (b) particle-size distribution graph, (c) activity plot (c.f. Skempton 1953) of the relationship between plasticity index (I_p) and clay fraction, (d) SEM image of pyrite (py) and sphalerite (sp) caused by dissolution, (e) desiccation cracks due to clay shrinkage post-deposition of mud volcano.

Blouin 2019), show proportions of silt and clay that are broadly similar to material from the Waimata Valley MV. The main particle fraction composing the mud is rich in clays (particularly in smectite), which leads to the conclusion that the stratigraphic source of the MV is probably within a clay-rich, low-permeability interval at depth (Yassir 1989; Kopf 2002). Indeed, at the Waimata MV, as with other MVs in the region (e.g. Ridd 1970), the source beds are a typically early Tertiary smectite-rich muds from beneath a cover of late Tertiary sedimentary rocks (e.g. Ridd 1970, p. 601). The results here have shown that the sampled muds exhibit high plasticity and are ‘active’ to ‘highly active’ (e.g. Skempton 1953). These plasticity values and material properties are not, however, assumed to be representative of all MVs, with many MVs globally showing a varied mineralogy and a medium plasticity (Yassir 1989).

Following the eruption and emplacement of the mud material, the mechanisms and likelihood of reactivation and remobilization are important to consider in terms of possible geohazard. The residual shear strength of the MV material ($S_d = 2\text{--}17 \text{ kPa}$) provides some insight into possible failure mechanisms and hazards from reactivation and flow. Friction angles measured in this study (mean 12.4°), exceed the topographic gradient of the MV surface, from the vent to distal deposition lobes. Nevertheless, in northeastern New Zealand, even on such shallow gradients, rainfall-induced failure and flow of surface soils can occur (Trotter 1993; Crozier

2010). Typically, pronounced desiccation of clay-rich soils occurs over the summer months, leading to formation of vertical fissures. The soil mass is then vulnerable to sudden and large rainfall events, with water infiltrating deeper and faster than when soils are moister and fissures have narrowed (Garrill *et al.* 2021). Once critical porewater pressures are reached, clayey soils lose their structure and cohesion, and fail. Often, like the Waimata MV, such earthflows and mudflows occur in sparsely-populated areas. However, many of these events can impact productive land, affect infrastructure such as roads and bridges, inflicting damage (Trotter 1993; Mazengarb and Speden 2000). An additional factor affecting the residual strength of soils is temperature, and this remains poorly understood (Bucher 1975). From ring shear tests at slow shearing rates, Shibasaki *et al.* (2017) found that in smectite-rich soils, decreases in ground temperature lowered shear resistance, triggering failure and initiating creep. In contrast, under relatively high shearing rates, strength was gained as temperature decreased. Thus, following eruption, the effects of temperature on the engineering stability of MV sediments is likely to be determined by a delicate balance of temperature and shearing rate, where episodic MV activity and warm fluid extrusion may control stability.

The LA-ICPMS analyses of four samples of separated clay-sized particles from the four sampled MVs contain significantly higher concentrations of Sr (140–505 ppm; mean 345 ppm) when

compared to clays from local clay-rich geological formations (30–137 ppm; mean 80 ppm). Other analysed trace elements have similar abundances between the MV and catchment samples. Strontium is typically associated with plagioclase feldspars, substituting easily for Ca in the mineral structure. However, Ca contents in all sampled clay-size fractions are generally low with no discernible difference between the MV clays and other catchment clays indicating plagioclase feldspar is not controlling variations in Sr content. Similarly, Eu which typically forms a 2+ cation and is also readily incorporated in plagioclase feldspar, shows no significant enrichment or correlation to Sr. Alternatively, Sr has a higher adsorption affinity with montmorillonite than with kaolinite due to differences in the mineral structure (Erten *et al.* 1988; Bascetin and Atun 2006). Smectite was identified as the main clay species by SEM in the Waimata Valley MV and thus high Sr in the clay size fraction may reflect the dominance of smectite clays. This also suggests that (1) smectite is not the dominant clay in other catchment samples, or (2) Sr has desorbed from the clay with transport away from the mud volcanoes.

Eruption event and geomorphology

Prior to the present study, the September 1994 MV eruption at the Brookby gas seep, Hawkes Bay, was the most recent and comprehensive study of a MV eruption within the East Coast Basin of New Zealand's North Island (Pettinga 2003). The interpreted eruption cycle at Brookby commenced with the rapid development (<1 h) of a mud dome *c.* 35 m in diameter and *c.* 2–3 m in height with a mudflow extending *c.* 180 m downslope from the seep. The permanent gas seep was within a 'floater' block within the melange zone. The mud that formed the eruption and mudflow, migrated upward along the contact between the floater block and the surrounding mélange (Pettinga 2003). Pettinga (2003, p. 118) characterized this MV as resulting from a diatreme (pillar-shaped vertical pipe characterized by rapid fluid advection; Brown 1990), rather than from a mud diapir (driven by buoyancy caused by bulk density contrasts; Brown 1990).

The morphology of MVs is variable and reflects the numerous properties that control the mechanisms of eruption/erosion (Mazzini and Etiopic 2017), including a range of dynamic and mechanical factors, in particular the viscosity of the ejected material. Indeed, the more fluid the material, the more likely the material is to flow and expand around the seep point. In contrast, more viscous material (less water, more sand-sized fraction) will lead to steep slopes and cones (e.g. Koturdag mud volcano, Azerbaijan; Aliyev *et al.* 2002). Also, gas-dominated eruptions can be powerful and short-lived, but have the power to disperse mud breccia over broader areas resulting a blocky morphology. Conversely, smooth or flat and laterally extensive morphologies originate from frequent water-dominated eruptions. The width of the shallow conduit is also important (a wider conduit tends to disperse the overpressure over a broader area), as is the source depth of the upwelling. Finally, pre-existing local topography also controls the geomorphology of the MV (e.g. Onderdonk *et al.* 2011). The December 15 2018 Waimata Valley MV eruption lasted only a few hours, was not preceded by earthquakes, and included expulsion of mud bombs, and a mud flow that extended across 11 500 m². Flow rate would have been enhanced by the domed topography, a product of uplift from the September 2016 Te Araroa earthquake (Fig. 2a). Indeed, the 2016 uplift and fracturing provided the pre-conditions for the 2018 MV formation, and its possible without this 2016 deformation, the MV would not have occurred at this location. The central area has a 'pie-shaped' morphology following the classification scheme of Mazzini and Etiopic (2017). Local MVs provide context for the eruption event and resulting geomorphology. While several MV eruptions have been recorded in the Waimata Valley and broader area since

1901, the December 15 2018 MV occurred from a completely new eruptive centre. Its eruptive activity started at around 8am and ended by early afternoon (Jim and Sharon Hall, farm owners, pers. comm. 2019). In contrast, activity at the Arakihi Road MV 600 m to the NW, and intersected by the same fault, has not been paroxysmal. Indeed, the Arakihi Road MV is characterized by an area of gently extruding gryphon-like (e.g. Mazzini and Etiopic 2017) mud cones <0.3 m high, across 9000 m² of bare ground (Ridd 1970). At the top of gryphons are small craters of muddy, cool, saline water through which methane intermittently bubbles (e.g. Ridd 1970). Following Mazzini and Etiopic (2017, p. 83), this style of activity is typical of 'dormant/sleeping' MVs, while Kopf (2002, p. 43) refers to the Arakihi Road MV as 'active'. Notwithstanding the terminology regarding the eruptive status of Arakihi Road MV, contrasting violent eruptions have been observed at the Mangaehu Stream MV (3.5 km SW of Waimata Valley MV) since 1901, although activity decreased in the latter part of the twentieth century (Ridd 1970). The eruption of July 25 1908 lasted 1 hour, accompanied by noise audible in the Waimata Valley, reported by Adams (1908, p. 98) to have resembled the 'snorting of a huge beast'. Adams (1908) estimated that debris was ejected to a height of 75–90 m. Strong (1931) reported that during the same eruption, debris was thrown to a height of 120 m and 0.25 kg boulders to a lateral distance of 128 m, and a 3.5–4 m thick mud sheet covered 40 000 m². No seismic activity was reported around the time of the 1908 event (Ridd 1970). The 6 May 1930 Mangaehu Stream MV eruption occurred at 4.30am when inhabitants of Waimata Valley to the east were awoken by rumbling noises, but again, no seismic activity was reported on that day, although earthquakes were of sufficient magnitude to be felt throughout Gisborne region over the following days (Ridd 1970). A mud sheet covering approximately the area of the 1908 was deposited, with an average depth of 1.5 m (Strong 1931). Most recently (10 December 2021), a small (*c.* 50 m diameter) mud volcano erupted 2.8 km of the Waimata Valley MV, in Mangaehu Stream over a period of one hour (Sharpe 2021), throwing rocks 50 m into the air, with the event clearly preceded by a swarm of M1.5–2.5 earthquakes at shallow depths in the days prior to the eruption (www.geonet.org.nz). Such earthquakes are only apparent on seismic recordings (Thouvenot and Bouchon 2008), and similar events would not have been noticed by laypeople prior to the 1908 or 1930 eruptions. Thus, the Mangaehu Stream MVs show similarities in terms of geomorphology and eruptive style to the Waimata Valley MV, but the 2018 Waimata Valley MV was not preceded by earthquakes. Also, the Arakihi Road MV close to, and along the same fault line as the Waimata Valley MV, displays clear geomorphological contrasts to the Waimata Valley MV.

Development of instability

Mud volcano activity has been closely linked to earthquakes in the region in the past (e.g. Ridd 1970; Sharpe 2021; www.geonet.org.nz) and globally (Mazzini and Etiopic 2017), but seismicity did not closely precede or coincide with the December 2018 Waimata Valley MV eruption. Rather, the M_w7.1 2016 Te Araroa earthquake caused uplift along the fault in the location where the MV erupted >2 years later. In the two years preceding the eruption, the Makarori geodetic monitoring station (www.geonet.org.nz), located *c.* 18 km to the SE (Fig. 1b), recorded gradual uplift of *c.* 15 mm, terminating around December 2018 (Fig. 7). Gradual subsidence has proceeded in the region since then. Although no geophysics or deep boreholes exist in the immediate vicinity of the Waimata Valley MV, the uplift-eruption-subsidence pattern accord with diapiric activity (Ridd 1970) or with the presence of a shallow mud chamber/reservoir (e.g. Mazzini and Etiopic 2017).

Another factor contributing to overpressure changes and the Waimata MV eruption may relate to slow slip earthquakes events

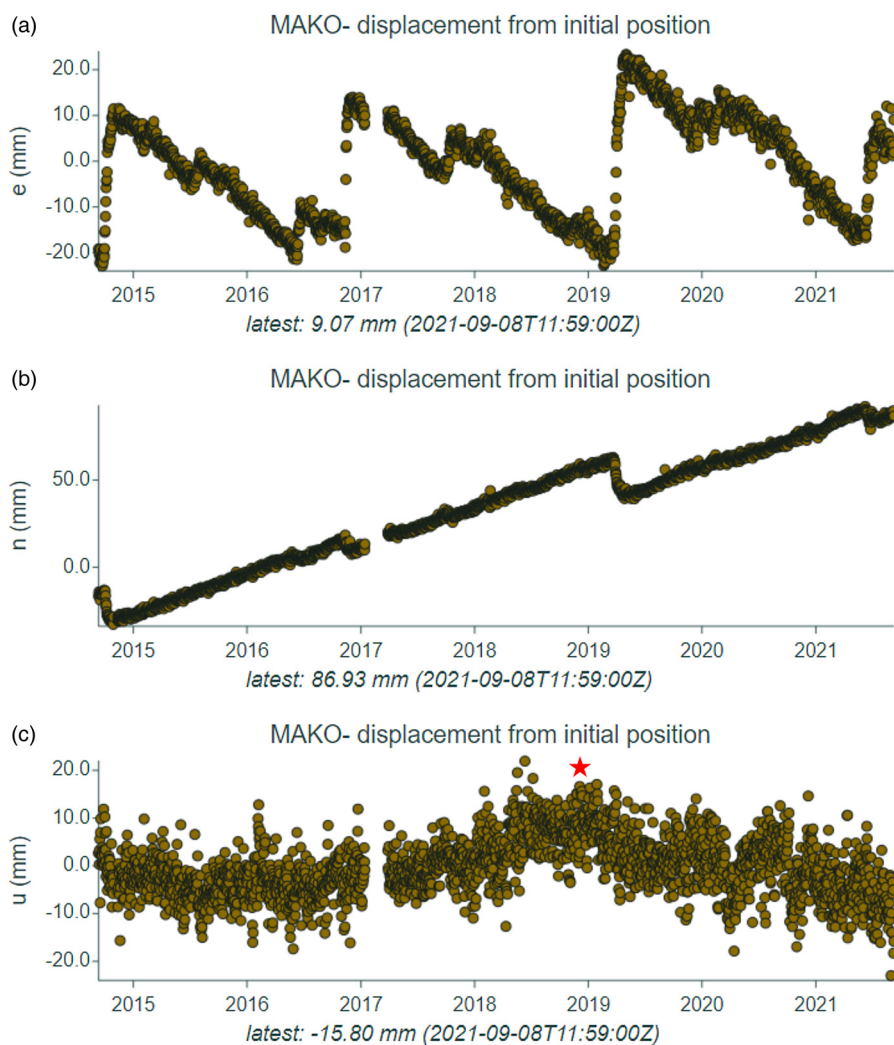


Fig. 7. Geodetic time series from the Makarori GNSS monitoring station (Fig. 1b), 18 km south of the study area (<https://www.geonet.org.nz>): (a) eastings showing periodic 2–6 week long, c. 40 mm slow slip events (SEEs), (b) northings, (c) gradual c. 15 mm uplift from 2017 until the 15 December 2018 Waimata MV eruption (red star), followed by subsidence. Gradual vertical displacement (u), peaked in December 2018, highlighted by red star, coinciding with 15 December 2018 MV eruption. Following the eruption, a slow slip event commenced the following month.

(SEEs; Barnes *et al.* 2020). This is a completely new slip mechanism that has been discovered, in which slip occurs faster than the plate motion rate, but too slowly to produce seismic waves. These have been identified within the Hikurangi subduction zone at shallow (<15 km) depths, and from continuous geodetic measurements recur every 1 to 2 years and last a duration of 2–6 weeks (Fig. 7a; Barnes *et al.* 2020). While no clear relationship exists in the geodetic data in Figure 7, a slow slip event (SEE) initiated within c. 6 weeks following the 15 December 2018 MV eruption (Fig. 7a, b). Thus, fluid build-up at shallow depths (<3 km deep) causing MV instability and fluid escapes may also be linked to deeper fluids related to the slow slip events (SEEs).

The fault that intersects both the Waimata Valley MV and the ‘dormant’ Arakihi Road MV is interpreted to have formed as a result of diapiric activity and intersects the Waimata Valley fault line further south (Ridd 1970; Neef and Bottrill 1992). The diapir source sediments in the region are associated with Paleocene/Eocene units such as the Mangatū Group, and high angle reverse faults (Ridd 1970) with these parent beds of smectite-rich clay from depths of up to 3000 m. Borehole observations in the Gisborne area show that the internal zones of mud diapirs are commonly overpressured, with overburden to fluid pressure ratios of 0.8–0.9 (Ridd 1970), though confining stress and shear stress will vary both laterally and vertically through a diapir (Brown 1990; Mazzini and Etiopic 2017). The area of the Waimata Valley MV is thought to represent one such diapiric inlier, and a conceptual formation model is shown in Figure 8. Following the deposition of these passive-margin clay-

bearing sediments, tectonic activity reactivated, and Paleogene sediments were rapidly buried under a thick sequence of Miocene sediments (i.e. Tolaga Group), followed by ongoing folding and faulting (Mazengarb and Speden 2000). Rapid burial of these passive-margin sediments is inferred to have created low-density sequences at depth, as the porewater was unable to escape due to their inherent low permeability. This ‘compaction disequilibrium’ can lead to both overpressure build-up in clay-rich layers, and undercompaction (thus low-density; Revil 2002). This can cause the low-density layers at depth (e.g. 3 km) to become buoyant (Fig. 8a), and particularly if tectonic weakening of the capping layer occurs, diapirism is initiated (Kopf 2002; Deville 2009; Mazzini and Etiopic 2017). The overpressure can be accentuated by (1) impermeable capping layers, (2) volumetric expansion due to the generation of hydrocarbons from kerogens and microbial activity or gas exsolution and expansion, and (3) dehydration reactions (i.e. illitization of clay minerals; Mazzini and Etiopic 2017). The diapir continues to ascend upwards from c. 3000 m depth along faults (c.f. Sibson 2003) proceeding due to gas expansion during rising, leading to further density lowering of the mud, to a shallow critical depth (<100 m; Fig. 2b). At that depth, the diapir ‘piercement’ meets pressurized fluids in reservoirs and fractures, causing increasing overpressure, promoting hydrofracturing and brecciation of surrounding units (e.g. Kopf 2002). At this threshold depth fracturing and breaching of the uppermost units occurs, sometimes facilitated by external factors such as earthquakes (Madonia *et al.* 2011), in this case, the 2016 Te Araroa Earthquake (Fig. 8c).

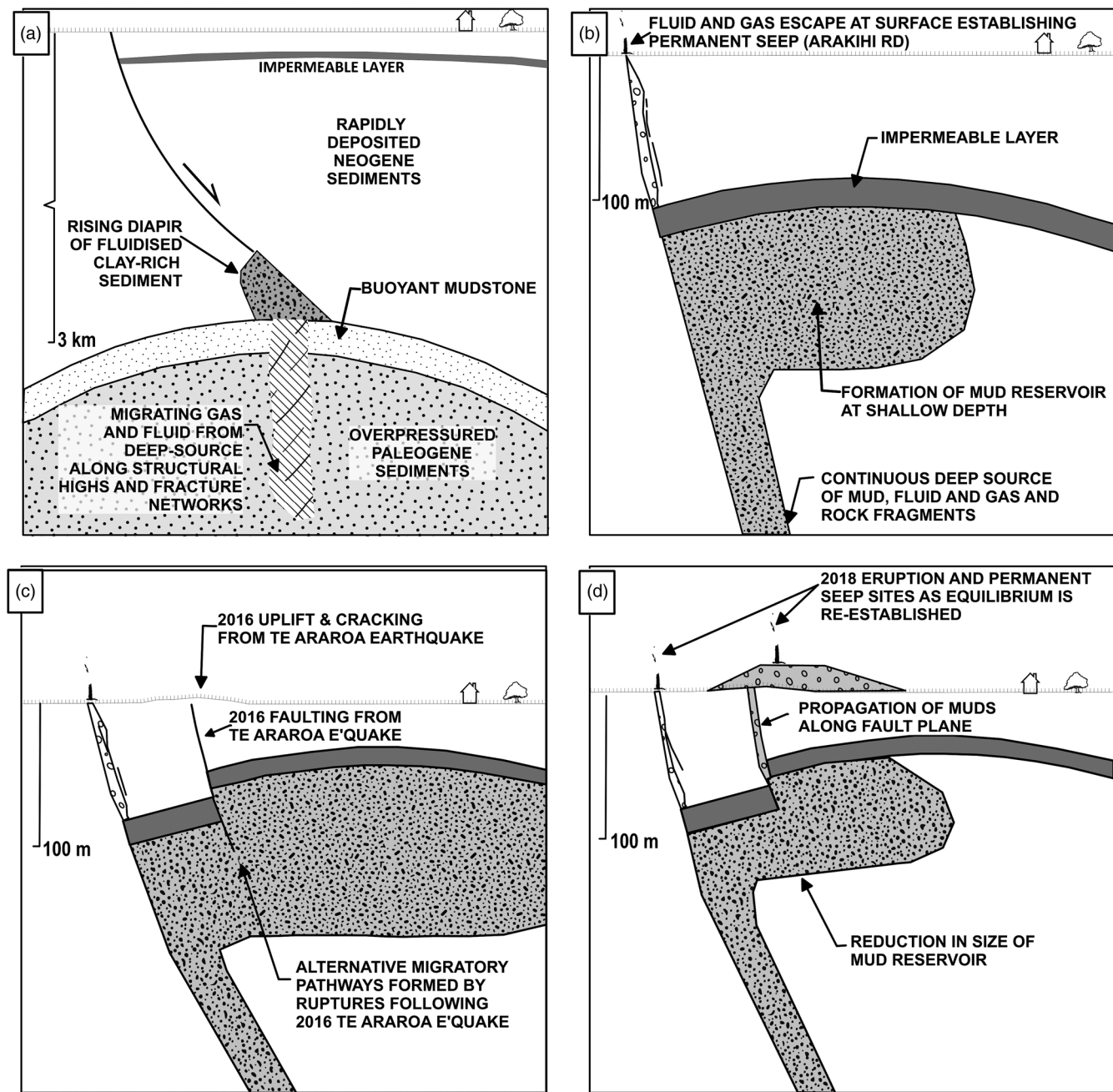


Fig. 8. Conceptual model of the 2018 Waimata Valley MV eruption (note indicative depth differences between A and B–D): (a) Diapir initiation, (b) formation of mud reservoir at shallow depth, (c) faulting effects of 2016 Te Araroa Earthquake, (d) 2018 mud volcano eruption and re-establishment of reservoir equilibrium and future activity. Diagrams not to scale.

Finally, eruption occurs (Fig. 8d), forming a mud volcano, and permanent seep sites as equilibrium is re-established, together with a reduced mud reservoir volume.

Conclusions

This work has provided a case study overview of soil index and geotechnical properties of recently erupted mud volcano (MV) material in the onshore Hikurangi margin, northeastern New Zealand. The MV formed within an existing region of mud volcanism, known to have erupted periodically since 1908. The formation of the 15 December 2018 Waimata Valley mud volcano has provided a rare and valuable reconnaissance opportunity to gain a better understanding of the processes and mechanisms associated with the mobilization of Eocene age deeply-buried sediments toward the surface. This was primarily achieved through an

engineering geological investigation of the site and analysis of the associated, highly plastic, smectite-rich materials. A conceptual model was developed as a representation of the likely process mechanism of mud volcano formation. While the eruption of many other MVs globally is associated by seismic activity, the December 2018 eruption was not coincident with seismicity. Nevertheless, the 2 September 2016 Te Araroa earthquake (M_w 7.1) caused significant ground deformation (ground cracking and uplift) at the location of the subsequent MV eruption. Indeed, the eruption coincides with the surface trace of a fault on which the Arakihi Road MV is located, 600 m to the NW. This highlights the importance of faulting in facilitating the eruption of diapiric muds in the region. The spatial coincidence of faults and Eocene mud rocks are important factors that should contribute to geohazard zonation, ahead of residential planning decision-making. Soil index properties, geochemical analysis and monitoring of geodetic data are useful methods in

this regard. Indeed, the geodetic data indicated that a two-year period of gradual regional uplift culminated with the eruption, followed by subsidence. This was then followed by the commencement of a slow-slip event (SSE). Hence, pre-conditioning factors are seemingly important, and this highlights the utility of an integrated approach to studying mud volcano phenomena in the region, using remote sensing and monitoring technology. Moreover, the relationship between uplift, MV activity, and slow slip events in the region warrants further study for geohazard mitigation.

Acknowledgements The Utting and Hall families are thanked for allowing access and information about the eruption. The fieldwork and laboratory analyses undertaken by students AL and AS was supported by the University of Auckland. Technical staff including Dave Wackrow, Brendan Hall, Catherine Hobbs, Stuart Morrow and Jeff Melster are thanked for their expertise. We acknowledge the New Zealand GeoNet project and its sponsors EQC, GNS Science, LINZ, NEMA and MBIE for providing data/images used in this study in Figure 7 (<https://www.geonet.org.nz/policy>).

Author contributions **AL:** formal analysis (lead), investigation (lead), writing – original draft (lead); **MSB:** conceptualization (equal), formal analysis (supporting), investigation (supporting), methodology (supporting), supervision (lead), validation (supporting), visualization (supporting), writing – original draft (supporting), writing – review & editing (lead); **MC:** conceptualization (equal), investigation (supporting), project administration (supporting), supervision (supporting), writing – review & editing (supporting); **MCR:** formal analysis (equal), investigation (supporting), methodology (equal), software (equal), writing – review & editing (equal); **AS:** data curation (supporting), formal analysis (equal), investigation (supporting), methodology (supporting); **JFT:** conceptualization (supporting), investigation (supporting), methodology (supporting), supervision (supporting), writing – review & editing (equal)

Funding This research received no specific grant from any funding agency in the public, commercial, or not-for-profit sectors.

Competing interests The authors declare that they have no known competing financial interests or personal relationships that could have appeared to influence the work reported in this paper

Data availability All data generated or analysed during this study are included in this published article (and if present, its supplementary information files).

Scientific editing by Cherith Moses; Michael Davies

References

- Adams, J.H. 1908. The eruption of the Waimata mud spring. *New Zealand Mines Record*, **12**, 97–101.
- Aliyev, A.A., Guliyev, I.S. and Belov, I.S. 2002. *Catalogue of Recorded Eruptions of Mud Volcanoes of Azerbaijan for a Period of Years 1810–2001*. Nafta Press, Baku, Azerbaijan.
- Barnes, P.M., Lamarche, G. et al. 2010. Tectonic and geological framework for gas hydrates and cold seeps on the Hikurangi subduction margin, New Zealand. *Marine Geology*, **272**, 26–48, <https://doi.org/10.1016/j.margeo.2009.03.012>
- Barnes, P.M., Wallace, L.M. et al. 2020. Slow slip source characterized by lithological and geometric heterogeneity. *Science Advances*, **6**, <https://doi.org/10.1126/sciadv.ayy3314>
- Bascetin, E. and Atun, G. 2006. Adsorption behavior of strontium on binary mineral mixtures of montmorillonite and kaolinite. *Applied Radiation and Isotopes*, **64**, 957–964, <https://doi.org/10.1016/j.apradiso.2006.03.008>
- Blott, S.J., Croft, D.J., Pye, K., Saye, S.E. and Wilson, H.E. 2004. Particle size analysis by laser diffraction. *Geological Society, London, Special Publications*, **232**, 63–73, <https://doi.org/10.1144/GSL.SP.2004.232.01.08>
- Blouin, A. 2019. *Mud Generation from Stratified Sediments in a Context of Mud Volcanism: The Role of Gas*. PhD thesis, Earth Sciences, University of Pau and the Adour Region.
- Blouin, A., Sultan, N., Callot, J.-P. and Imbert, P. 2019. Sediment damage caused by gas exsolution: a key mechanism for mud volcano formation. *Engineering Geology*, **263**, 105313, <https://doi.org/10.1016/j.enggeo.2019.105313>
- Brown, K.M. 1990. The nature and hydrogeologic significance of mud diapirs and diatremes for accretionary systems. *Journal of Geophysical Research*, **95**, 8969–8982, <https://doi.org/10.1029/JB095iB06p08969>
- BS 1377-2 1990. *Methods of test for soils for civil engineering purposes - classification tests*.
- Bucher, F. 1975. *Die Restscherfestigkeit Natürlicher Böden, ihre Einflussgrößen und Beziehungen als Ergebnis experimenteller Untersuchungen*. Institutes für Grundbau und Bodenmechanik Eidgenössische Technische Hochschule, Zürich, Report No. **103**.
- Chen, J., Song, H. et al. 2015. Morphologies, classification and genesis of pockmarks, mud volcanoes and associated fluid escape features in the northern Zhongjia Basin, South China Sea. *Deep-Sea Research II*, **122**, 106–117, <https://doi.org/10.1016/j.dsr.2015.11.007>
- Crozier, M. 2010. Landslide geomorphology: an argument for recognition, with examples from New Zealand. *Geomorphology*, **120**, 3–15, <https://doi.org/10.1016/j.geomorph.2009.09.010>
- Deville, É. 2009. Mud volcano systems. In: Lewis, N. and Moretti, A. (eds) *Volcanoes: Formation, Eruptions and Modelling*. Nova Science Publishing, 95–126.
- Deville, E., Battani, A. et al. 2003. The origin and processes of mud volcanism: new insights from Trinidad. *Geological Society, London, Special Publications*, **216**, 475–490, <https://doi.org/10.1144/GSL.SP.2003.216.01.31>
- Dimitrov, L.I. 2002. Mud volcanoes—the most important pathway for degassing deeply buried sediments. *Earth Science Reviews*, **59**, 49–76, [https://doi.org/10.1016/S0012-8252\(02\)00069-7](https://doi.org/10.1016/S0012-8252(02)00069-7)
- Erten, H.N., Aksoyoglu, S., Hatipoglu, S. and Gokturk, H. 1988. Sorption of Cesium and Strontium on Montmorillonite and Kaolinite. *Radiochimica Acta*, **44–45**, 147–151, <https://doi.org/10.1524/ract.1988.4445.1.147>
- Etiopic, G. 2015. *Natural Gas Seepage*. Springer International Publishing, Switzerland.
- Field, B.D., Uruski, C.I. et al. 1997. *Cretaceous-Cenozoic geology and petroleum systems of the East Coast Region, New Zealand*. Institute of Geological and Nuclear Sciences Monograph, **19**. Institute of Geological and Nuclear Sciences Ltd, Wellington, New Zealand.
- Gabr, M.A., Coonse, J. and Lambe, P.C. 2001. A potential model for compaction evaluation of piedmont soils using dynamic cone penetrometer (DCP). *Geotechnical Testing Journal*, **24**, 308–313, <https://doi.org/10.1520/GTJ11349>
- Garrill, R., Grieve, S., George, A., Richards, N. and Brook, M. 2021. Monitoring slope instability during reinstatement of State Highway 11 at Lemon's Hill (35 degrees S), Northland, New Zealand. *Australian Geomechanics*, **56**, 159–168.
- Gibo, S., Egashira, K. and Ohtsubo, M. 1987. Residual strength of smectite-dominated soils from the Kamenose landslide in Japan. *Canadian Geotechnical Journal*, **24**, 456–462, <https://doi.org/10.1139/t87-057>
- Guliyev, I.S., Feizulayev, A.A. and Huseynov, D.A. 2001. Isotope geochemistry of oils from fields & mud volcanoes in the South Caspian Basin, Azerbaijan. *Petroleum Geoscience*, **7**, 201–209, <https://doi.org/10.1144/petgeo.7.2.201>
- James, M.R., Robson, S., d’Oleire-Oltmanns, S. and Niethammer, U. 2017. Optimising UAV topographic surveys processed with structure-from-motion: ground control quality, quantity and bundle adjustment. *Geomorphology*, **280**, 51–66, <https://doi.org/10.1016/j.geomorph.2016.11.021>
- Judd, A. and Hovland, M. 2007. *Seabed Fluid Flow, the Impact on Geology, Biology and the Marine Environment*. Cambridge University, Cambridge.
- Kopf, A.J. 2002. Significance of mud volcanism. *Review of Geophysics*, **40**, 1–52, <https://doi.org/10.1029/2000RG000093>
- Kopf, A., Delisle, G., Faber, E., Panahi, B., Aliyev, C. and Guliyev, I. 2010. Long-term in situ monitoring at Dashgil mud volcano, Azerbaijan: a link between seismicity, porepressure transients and methane emission. *International Journal of Earth Science*, **99**, 227–240, <https://doi.org/10.1007/s00531-009-0487-4>
- Madonia, P., Grassi, F., Cangemi, M. and Musumeci, C. 2011. Geomorphological and geochemical characterisation of the 11 August 2008 mud volcano eruption at S. Barbara village (Sicily, Italy) and its possible relationship with seismic activity. *Natural Hazards and Earth System Sciences*, **11**, 1545–1557, <https://doi.org/10.5194/nhess-11-1545-2011>
- Magoon, L.B. and Schmoker, J.W. 2000. The Total Petroleum System - the natural fluid network that constrains the assessment units. In: *World Energy Assessment Team, U.S. Geological Survey World Petroleum Assessment 2000 - Description and Results*.
- Mazengarb, C. and Speden, I.G. 2000. *Geology of the Raukumara Area: Scale 1:250,000*. Institute of Geological and Nuclear Sciences 1:250,000 Geological Map, **6**, Lower Hutt.
- Mazzini, A. and Etiopic, G. 2017. Mud volcanism: an updated review. *Earth-Science Reviews*, **168**, 81–112, <https://doi.org/10.1016/j.earscirev.2017.03.001>
- Mazzini, A., Nermoen, A., Krotkiewski, M., Podladchikov, Y., Planke, S. and Svensen, H. 2009. Strike-slip faulting as a trigger mechanism for overpressure release through piercement structures. Implications for the Lusi mud volcano, Indonesia. *Marine and Petroleum Geology*, **26**, 1751–1765, <https://doi.org/10.1016/j.marpetgeo.2009.03.001>
- Meehan, C.L., Brandon, T.L. and Duncan, M. 2007. Measuring drained residual strengths in the bromhead ring shear. *Geotechnical Testing Journal*, **30**, 466–473, <https://doi.org/10.1520/GTJ101017>
- Milkov, A.V. 2000. Worldwide distribution of submarine mud volcanoes and associated gas hydrates. *Marine Geology*, **167**, 29–42, [https://doi.org/10.1016/S0025-3227\(00\)00022-0](https://doi.org/10.1016/S0025-3227(00)00022-0)
- Neef, G. and Bottrill, R.S. 1992. The Cenozoic geology of the Gisborne area (1:50,000 metric sheet Y18AB), North Island, New Zealand. *New Zealand Journal of Geology and Geophysics*, **35**, 515–531, <https://doi.org/10.1080/00288306.1992.9514545>
- Nelson, C.S. and Healy, T.R. 1984. Pockmark-like structures on the Poverty Bay sea bed: possible evidence for submarine mud volcanism. *New Zealand Journal of Geology and Geophysics*, **27**, 225–230, <https://doi.org/10.1080/00288306.1984.10422530>

- NZGS 2001. *Guideline for Hand Held Shear Vane Test*. New Zealand Geotechnical Society Inc, Wellington
- NZGS 2005. *Field Description of Soil and Rock*. New Zealand Geotechnical Society Inc, Wellington
- Odonne, F., Impert, P. *et al.* 2020. Mud volcano growth by radial expansion: examples from onshore Azerbaijan. *Marine and Petroleum Geology*, **122**, 104051, <https://doi.org/10.1016/j.marpetgeo.2019.104051>
- Onderdonk, N., Mazzini, A., Shafer, L. and Svensen, H. 2011. Controls on the geomorphic expression and evolution of gryphons, pools, and caldera features at hydrothermal seeps in the Salton Sea geothermal field, southern California. *Geomorphology*, **130**, 327–342, <https://doi.org/10.1016/j.geomorph.2011.04.014>
- Pettinga, J.R. 2003. Mud volcano eruption within the emergent accretionary Hikurangi margin, southern Hawke's Bay, New Zealand. *New Zealand Journal of Geology and Geophysics*, **46**, 107–121, <https://doi.org/10.1080/00288306.2003.9514999>
- Revil, A. 2002. Genesis of mud volcanoes in sedimentary basins: a solitary wave-based mechanism. *Geophysical Research Letters*, **29**, <https://doi.org/10.1029/2001GL014465>
- Ridd, M.F. 1970. Mud Volcanoes in New Zealand. *American Association of Petroleum Geologists Bulletin*, **54**, 601–616.
- Roberts, R.C., Fairclough, T., Hargraves, S., Cassidy, G., Wahab, H. and Stannard, M. 2017. A ground investigation specification for New Zealand. Proceedings of the 20th New Zealand Geotechnical Society Symposium, 24–26 November, Napier.
- Sharpe, M. 2021. *Mud volcano erupting on Gisborne farm threw large rocks 50 metres*. Retrieved from: <https://www.stuff.co.nz/science/127336946/mud-volcano-erupting-on-gisborne-farm-threw-large-rocks-50-metres>
- Shibasaki, T., Matsuura, S. and Hasegawa, Y. 2017. Temperature-dependent residual shear strength characteristics of smectite-bearing landslide soils. *Journal of Geophysical Research: Solid Earth*, **122**, 1449–1469, <https://doi.org/10.1002/2016JB013241>
- Sibson, R.H. 2003. Brittle-failure controls on maximum sustainable overpressure in different tectonic regimes. *American Association of Petroleum Geologists Bulletin*, **87**, 901–908, <https://doi.org/10.1306/01290300181>
- Skempton, A.W. 1953. The Colloidal activity of clays. Proceedings of the 3rd International Conference on Soil Mechanics and Foundation Engineering, Zurich, **1**, 57–61.
- Skempton, A.W. and Northery, R.D. 1953. The sensitivity of clays. *Geotechnique*, **3**, 30–53, <https://doi.org/10.1680/geot.1952.3.1.30>
- Standards Australia 2006. *AS 1289.3.8.1. Methods of Testing Soils for Engineering Purposes – Soil Classification Tests – Dispersion – Determination of Emerson Class Number of a Soil*. Standards Australia, Sydney, NSW.
- Stockwell, M. 1977. Determination of allowable bearing pressure under small structures. *New Zealand Engineering*, **32**, 132–135.
- Strong, S.W.S. 1931. Ejection of fault breccia in the Waimata Survey District, Gisborne. *New Zealand Journal of Science and Technology*, **12**, 257–267.
- Strong, S.W.S. 1933. The Sponge Bay uplift, Gisborne and the Hangaroa mud blowout. *New Zealand Journal of Science and Technology*, **15**, 76–78.
- Thouvenot, F. and Bouchon, M. 2008. What is the lowest magnitude threshold at which an earthquake can be felt or heard, or objects thrown into the air? In: Fréchet, J., Meghraoui, M. and Stucchi, M. (eds) *Historical Seismology: Interdisciplinary Studies of Past and Recent Earthquakes. Modern Approaches in Solid Earth Sciences*, **2**. Springer, Dordrecht, 313–326.
- Tingay, M., Manga, M., Rudolph, M.L. and Davies, R. 2017. An alternative review of facts, coincidences and past and future studies of the Lusi eruption. *Marine and Petroleum Geology*, **95**, 345–361, <https://doi.org/10.1016/j.marpetgeo.2017.12.031>
- Trotter, C.M. 1993. Weathering and regolith properties at an earthflow site. *Quarterly Journal of Engineering Geology*, **26**, 163–178, <https://doi.org/10.1144/GSL.QJEGH.1993.026.003.02>
- Vona, A., Giordanò, G., De Benedetti, A.A., D'Ambrosio, R. and Romano, C. 2015. Ascent velocity and dynamics of the Fiumicino mud eruption, Rome, Italy. *Geophysical Research Letters*, **42**, 6244–6252, <https://doi.org/10.1002/2015GL064571>
- Yassir, N.A. 1989. *Mud Volcanoes and the Behaviour of Overpressured Clays and Silts*. Unpublished Doctoral Thesis, University College London, London, United Kingdom.